Enhanced truss topology optimization (TTO) applied to a cellular wing box

Enrico Stragiotti, François-Xavier Irisarri, Cédric Julien, Joseph Morlier

Enhanced truss topology optimization (TTO) applied to a cellular wing box

Enrico Stragiotti*, François-Xavier Irisarri*, Cédric Julien*
ONERA - The French Aerospace Lab, 92320 Châtillon, France

and

Joseph Morlier†
ICA - Institut Clément Ader, 31400 Toulouse, France

Cellular architectured structures' most appealing characteristic is that they are able to create large structures assembling small repetitive components. Thanks to their modular nature, they bring interesting features among which reduced tooling, fast assembly, and short repair time. In the first part of the article, we formulate an optimizing method that minimizes the mass of a cellular architectured structure taking into account internal stresses, local buckling, and pattern repetition constraints. The proposed solving algorithm mitigates the appearance of local minima, a critical problem for discrete trusses. In the second part, the optimization method is applied to a real-size aeronautic application: the minimization of the mass of a cellular 3D wing box subject to lift and torsion loads. Compared to classic cell topologies, the proposed method found a cell 10-times lighter, at the cost of increased manufacturing difficulty.

I. Introduction

Assembled cellular ultralight structures present an opportunity to greatly improve the performance and cost efficiency of modern aerostructures[1]. The repetitive nature brings various interesting features among which reduced tooling, fast assembly, and short repair time. Additionally, as the mechanical performance of the structure is greatly influenced by the topology and the materials of the repetitive pattern, cellular structures are naturally prone to optimization for various scenarios.

In the structure optimization field periodic materials are often modeled by means of asymptotic homogenization[2]. The heterogeneous cell topology (or Representative Volume Element (RVE)) is treated as homogeneous material with associated mechanical properties i.e., equivalent elastic tensor, shear modulus, etc. The homogenization approach is valid only if the RVE contains enough information about the heterogeneous material and if the structure presents significant periodicity. When designing cellular structures (and not materials), no scale separation is assumed between the repetitive pattern and the structure itself. Consequently, the hypotheses of asymptotic homogenization are not always verified. For that reason, full-scale approaches[3] have been developed.

Among all the structure optimization methods, topology optimization allows achieving any shape within the design space instead of dealing with predefined configurations. Topology optimization considers the design domain as a continuum, in which each location may or may not have a material assigned to it. Even if the freedom of the design space offered by the continuum meshes is high, it is known that at very low volume fractions (ultralight structures) and, especially if buckling constraints and manufacturing consideration (minimum plate thickness) are taken into account, the optimal topology is a truss structure[4]. In addition to that, truss structure design naturally relies on constraints on maximum allowable stress, buckling, and maximum slenderness, which are all known for being difficult to implement on topology optimization using a Nested Analysis and Design (NAND) formulation[5]. On top of that, topology optimization proved to be extremely computation intensive, especially when optimizing large-scale 3D structures[6] with low volume fractions, even with adaptive meshes[7].

Building on a Simultaneous Analysis and Design (SAND) formulation, Truss Topology Optimization (TTO) is a structural optimization algorithm that finds a near-optimal truss structure with respect to a given load case. Instead of working with a continuous domain as topology optimization does, TTO optimizes the cross-sectional areas and the connectivity of the members of a discrete ground structure. In the early works, the TTO problem was formulated in terms of member forces[8] with plastic material formulation, ignoring the kinematic compatibility to

*DMAS - Département matériaux et structures, enrico.stragiotti@onera.fr
†ISAE - SUPAERO, joseph.morlier@isae-supaero.fr

obtain a Linear Programming (LP) problem. Formulated in that way, the problem becomes inexpensive to solve but loses in generality. One can solve only single load case problems for elastic design and is restricted to statically determinate structures or mechanism[9]. Aiming at mitigating these criticalities, TTO has been enriched with the kinematic compatibility constraint[10], and also local buckling[11] and global buckling[12] constraints.

The objective of the present research is to develop an optimizing algorithm to minimize the mass of an assembled cellular structure. The proposed formulation builds on the classic LP TTO optimization problem, adding the aforementioned kinematic compatibility and local buckling constraints. Furthermore, we enrich the formulation by imposing pattern repetition, implemented using the full-scale approach called variable linking[13]. The proposed formulation performance is evaluated on a simplified 3D wing box load case and benchmarked against classic cell topologies.

II. Cellular truss topology optimization

In this section, we propose a TTO formulation developed specifically to tackle the difficulties in optimizing 3D ultralight cellular structures with no scale separation between the repeating pattern and the structure. The objective we choose is the minimization of the mass constrained by stress, local buckling, and pattern repetition constraints. The optimized structure is achieved by modifying the cross-sectional area and the connectivity of a discrete mesh. TTO acts on a ground structure that is defined as a set of bar members that connect a grid of M pin-jointed points.

The proposed formulation is based on the SAND approach, where, in addition to the member cross-sectional areas, the member forces and the nodal displacements are used as state variables. Consequently, the equations of structural mechanics are imposed as constraints of the optimization problem and not explicitly solved as for NAND approaches. One of the advantages of SAND approach is that the state variables are independent of each other and, thus, the sensitivity calculation of the constraints functions is simpler.

The problem formulation is stated in terms of linked cross-sectional member areas $\boldsymbol{\kappa}$, member forces $\boldsymbol{q}$ and nodal displacements $\boldsymbol{U}$ as follows:

$$
\begin{aligned}
\mathbb{P}_1: \quad \min_{\boldsymbol{\kappa},\boldsymbol{q},\boldsymbol{U}} \quad & V = \boldsymbol{\ell}^{*T}\boldsymbol{a} && \text{(Volume minimization)} \\
\text{s.t.} \quad & \boldsymbol{B}\boldsymbol{q} = \boldsymbol{f} && \text{(Force equilibrium)} \\
& \boldsymbol{q} = \frac{\boldsymbol{a}E}{\boldsymbol{\ell}}\boldsymbol{b}^T\boldsymbol{U} && \text{(Compatibility constraints)} \\
& \boldsymbol{q} \geq -\frac{s\boldsymbol{a}^2}{\boldsymbol{\ell}^2} && \text{(Euler's buckling constraints)} \\
& \boldsymbol{a} = \boldsymbol{G} \otimes \boldsymbol{\kappa} && \text{(Variable linking)} \\
& -\sigma_C\boldsymbol{a} \leq \boldsymbol{q} \leq \sigma_T\boldsymbol{a} && \text{(Stress constraints)} \\
& \boldsymbol{\kappa} \geq 0, && \text{(Positive cross-sectional member areas)}
\end{aligned}
\tag{1}
$$

where $\boldsymbol{B}$ is a $2M \times N_{el}$ matrix containing the direction cosines of j-th member with respect to the i-th degree of freedom to calculate the nodal force equilibrium. M is the number of nodes and N_{el} the number of members of the ground structure. $\boldsymbol{q} = [q_1, q_2, \ldots, q_{N_{el}}]^T$ is the vector containing the internal member forces caused by the external load $\boldsymbol{f} = [f_1, f_2, \ldots, f_{2M}]^T$. The state variable $\boldsymbol{\kappa} = [\kappa_1, \kappa_2, \ldots, \kappa_{n_{el}}]^T$ represents the cross-sectional area of the n_{el} members of the repetitive cell and is linked to the structure cross-sectional member areas $\boldsymbol{a} = [a_1, a_2, \ldots, a_{N_{el}}]^T$ through the cellular mapping vector $\boldsymbol{G}$. σ_C and σ_T are the compressive and tensile maximum allowable stresses of the material, respectively. $\boldsymbol{b}$ represents the i-th column of $\boldsymbol{B}$, while s is a constant used for Euler buckling calculation that depend on the cross-section topology. Our optimization takes into account only the linear behavior of the structure.

The resolution of Problem $\mathbb{P}_1$ produces complex structures made up of a multitude of small members that resemble to Michell structures. Substituting in the volume evaluation function $V = \boldsymbol{\ell}^T\boldsymbol{a}$ the member physical length $\boldsymbol{\ell}$ with $\boldsymbol{\ell}^* = [\ell_1 + j_c \max(\boldsymbol{\ell}), \ell_2 + j_c \max(\boldsymbol{\ell}), \ldots, \ell_{N_{el}} + j_c \max(\boldsymbol{\ell})]^T$, one would penalize the appearance of small members[14]. $\boldsymbol{\ell}^*$ is called augmented member length and j_c is the joint cost. This approach permits avoiding the apparition of structures with tiny features when a fine ground structure is adopted.

The contributions of our studies is to revisit and enrich the classic LP TTO formulation[8]. The cellular nature of lattice structures is taken into account by implementing the full-scale method called variable linking. These constraints, together with local buckling and kinematic compatibility constraints are regrouped in a unique formulation, with the idea of minimizing the need for post-processing between the optimized structure and the manufacturing phase. The resulting formulation proved to be extremely prone to local minima, and therefore we suggest a two-step optimization algorithm to limit that negative behavior. All these additions, together with the resolution algorithm, will be detailed in the next sections.

A. Cell structure optimization

To take into account the cellular topology of the structure, the variable linking scheme is implemented on a structured grid. This approach is usually found in the topology optimization literature and is adapted here to work with TTO. The variable linking approach is a full-scale method with a repeated pattern i.e. no scale separation is assumed between the repetitive cell and the structure.

Let us take a 2D truss structure for convenience. It is made by M joints and partitioned into $N_c = N_{c,x} \times N_{c,y}$ repetitive cells (see Figure 1). Every cell is composed by $m = m_x \times m_y$ joints connected by $n_{el} = (m(m-1)/2)$ elements in the case of a fully-connected cell ground structure. We define $\boldsymbol{\kappa} = [\kappa_1, \kappa_2, \ldots, \kappa_{n_{el}}]^T$ as the linked cross-sectional area of the members defined in the design cell Ω_c. The optimization is conducted only on the repetitive design cell Ω_c, while the structural response and the sensitivity analysis are evaluated over the whole structure Ω.

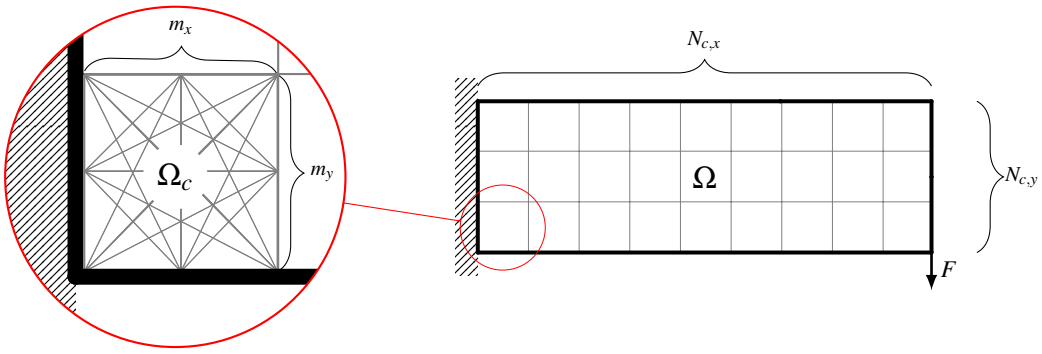

Figure 1: The variable linking scheme is applied to a cellular 2D structure. The design cell Ω_c represents the design space of the optimizer, and it is repeated over the structure domain Ω.

Variable $\boldsymbol{\kappa}$ is linked to the structure cross-sectional area $\boldsymbol{a}$ over the entire structure Ω using the following equation:

$$\boldsymbol{g}_{\text{cell}} := \boldsymbol{a} = \boldsymbol{G} \otimes \boldsymbol{\kappa} = \begin{bmatrix} G_1 \boldsymbol{\kappa} \\ \vdots \\ G_{N_c} \boldsymbol{\kappa} \end{bmatrix}, \tag{2}$$

where $\otimes$ stands for the Kroneker product. In the case of a single cell optimization, $\boldsymbol{G} = [G_1, G_2, \ldots, G_{N_c}] \in \mathbb{R}_c^N$ is defined as an all-ones vector of size N_c, $\boldsymbol{G} = [1, 1, \ldots, 1] \in \mathbb{R}_c^N$. The Kroneker product operation described above tiles the variable $\boldsymbol{\kappa}$ N_c-times. The Kronecker product is a linear operator and suitable for the sensitivity analysis of problem $\mathbb{P}_1$.

B. Kinematic compatibility constraints

To optimize cellular structures, that are usually statically indeterminate, or to solve multiple load cases, it is necessary to impose the kinematic compatibility constraints[15]. These equations restrict the displacement field $\boldsymbol{U}$ in such a way that strains and internal stresses comply with Hooke's law $\sigma_j = E_j \varepsilon_j$ with $j \in [1, 2, \ldots, N_{el}]$. Recalling that in a truss the relationship between nodal displacements and member deformations is $\boldsymbol{b}_j^T \boldsymbol{U} = \ell_j \varepsilon_j$, we can formulate the kinematic compatibility constraints $\boldsymbol{g}_{\text{comp}}$ as:

$$g_{j,\,\text{comp}} := \frac{a_j E_j}{\ell_j} \boldsymbol{b}_j^T \boldsymbol{U} - q_j = 0 \quad \forall j \in [1, 2, \ldots, N_{el}], \tag{3}$$

An advantage of using the kinematic compatibility constraints to impose the linear mechanical behavior with respect to solving a Finite Element Analysis (FEA) inside a NAND formulation is that the problem stays well-posed even if the section variables go to 0. As the linear system $\boldsymbol{K}\boldsymbol{U} = \boldsymbol{f}$ is never explicitly solved during the optimization, it is not necessary to impose a lower bound on these variables to avoid a singular stiffness matrix. Kinematic compatibility constraints are non-linear as the design variables $\boldsymbol{q}$ are dependent on $\boldsymbol{a}$ and $\boldsymbol{U}$.

C. Local buckling constraints

Adding local buckling constraints is fundamental as ultralight truss structures are often dominated by this mode of failure[4]. Using the notation of Achtziger[11], the Euler's buckling constraints $\boldsymbol{g}_{\text{buck}}$ are stated as:

$$g_{j,\,\text{buck}} := q_j + \frac{s a_j^2}{\ell_j^2} \geq 0 \quad \forall j \in [1, 2, \ldots, N_{el}], \tag{4}$$

where s is a parameter dependent of the member material and section topology. In this work we choose to use circular sections with $s = \pi E/4$.

Equation 4 is non-linear but still convex, and it would not create too many difficulties for a modern non-linear optimizer. The criticality is that by imposing local buckling constraints over a topology optimization problem (where the lower bound for the member section is 0), the optimization domain becomes disjointed[15]. This problem is made even worse as we introduce the non-linearities of the kinematic compatibility constraints.

D. Optimization algorithm

Directly solving Problem $\mathbb{P}_1$ using a Non-Linear Programming (NLP) solver systematically yields unsatisfying local minima. Getting rid of a member once the local buckling constraints are active proved to be challenging even for modern NLP solvers. The solutions are, thus, usually made by many intersecting thin bars. This behavior becomes even worse when a high number of cells is used.

Because of that, we propose a two-step optimization algorithm that aims at mitigating the proneness of the optimizer to get stuck on local minima. The steps are:

1. Problem $\mathbb{P}_1$ is relaxed: kinematic compatibility constraints are omitted and local buckling constraints are linearized. We call this relaxed problem $\mathbb{P}_2$. The solution to this Problem $\mathbb{P}_2$ proved to be less influenced by local minima as the response surface become smoother. Subsequently, the initial ground structure is simplified, removing all the members that do not appear in the relaxed problem solution.

2. The kinematic compatibility and the local buckling constraints are restored. Problem $\mathbb{P}_1$ is solved in its original form on the simplified ground structure. The initial values for the cross-sectional areas are the solutions of Problem $\mathbb{P}_2$.

The algorithm proposed to solve the ultralight cellular structure optimization is presented in Fig. 2.

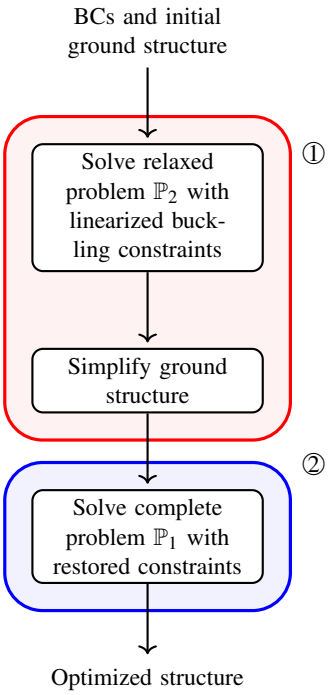

Figure 2: The proposed two-step optimization algorithm. In the first part, the solution of a relaxed problem is used to simplify the fully connected cell ground structure. In the second part, the complete problem with the restored constraints is solved on the simplified ground structure.

While there is no mathematical guarantee that the optimized point found following this method is the global optimum of the NLP problem, we systematically find better results using this approach instead of directly solving $\mathbb{P}_1$.

Let us break down the algorithm presented in Fig. 2 and explicate all the phases in detail. Taking as input the boundary conditions (physical dimensions) and the cell parameters (number of repetitive cells and number of nodes per dimension), the first step is to generate the initial ground structure. The optimal structure is searched

in a subset of this discretization. This step is critical as the solution is highly dependent on the initial ground structure[12].

In our work, we consider a fully-connected ground structure for every cell of the structure. This promotes the exploration of new cell topologies. These distinct ground structures are then assembled based on the cell parameters of the structure. Therefore, in the final structure, each cell contains its own members, and there are no members spanning over multiple cells. Overlapped members on the cell edges are kept during the optimization and their area is summed at the end.

Once the ground structure is defined, it is possible to iteratively solve the relaxed problem $\mathbb{P}_2$ with linearized buckling constraints. The local buckling formula is linearized for every j member in the neighborhood of a_j^0 using a first order Taylor expansion[16]:

$$\tilde{q}_{cr,j} = q_{cr,j}(a_j^0) + (a_j - a_j^0)\left.\frac{\partial q_{cr,i}}{\partial a}\right|_{a=a_j^0} \tag{5}$$

where $q_{cr,j}(a_j^0)$ represents the Euler's critical load of the j-th bar with cross-sectional area a_j^0.

The linearized Euler buckling constraints the Euler's buckling constraints $\tilde{\boldsymbol{g}}_{\text{buck}}$ are stated as:

$$\tilde{g}_{j\,\text{buck}} := q_j \geq \tilde{q}_{cr,i} = -\frac{s a_j^0 \left(2a_j - a_j^0\right)}{\ell_j^2} \quad \forall j \in [1,2,\ldots,N_{el}], \tag{6}$$

where superscript $\sim$ indicates linearized variables.

We can now state the relaxed Problem $\mathbb{P}_2$ in terms of linked cross-sectional member areas $\boldsymbol{\kappa}$ and member forces $\boldsymbol{q}$ as:

$$\begin{aligned}
\mathbb{P}_2: \quad \min_{\boldsymbol{\kappa},\boldsymbol{q}} \quad & V = \boldsymbol{\ell}^{*T}\boldsymbol{a} && \text{(Volume minimization)}\\
\text{s.t.} \quad & \boldsymbol{B}\boldsymbol{q} = \boldsymbol{f} && \text{(Force equilibrium)}\\
& \boldsymbol{q} \geq -\frac{s\boldsymbol{a}^0\left(2\boldsymbol{a}-\boldsymbol{a}^0\right)}{\boldsymbol{\ell}^2} && \text{(Euler's buckling constraints)}\\
& \boldsymbol{a} = \boldsymbol{G}\otimes\boldsymbol{\kappa} && \text{(Variable linking)}\\
& -\sigma_C\boldsymbol{a} \leq \boldsymbol{q} \leq \sigma_T\boldsymbol{a} && \text{(Stress constraints)}\\
& \boldsymbol{\kappa} \geq 0. && \text{(Positive sections)}
\end{aligned} \tag{7}$$

As the objective function and the constraints are all linear, the problem can be iteratively solved by the means of Sequential Linear Programming (SLP) algorithm until convergence. The logic of the SLP algorithm is presented in Fig. 3.

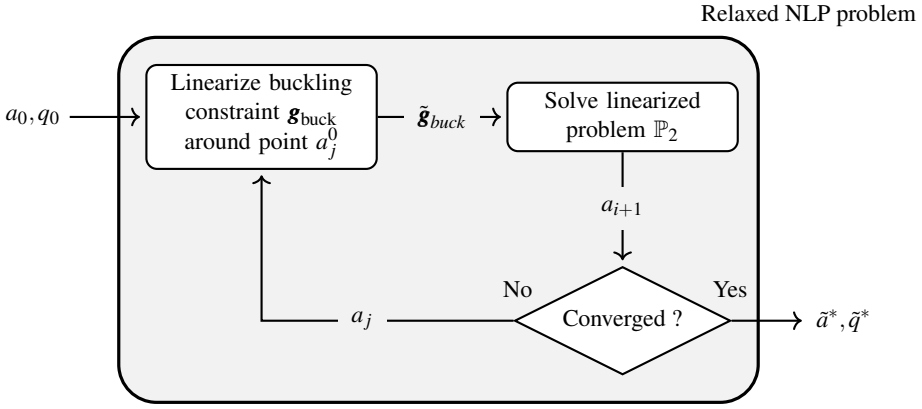

Figure 3: Relaxed NLP resolution flowchart using an SLP formulation.

The gradient of Eq. 6 goes to zero when a member is removed from the topology i.e., member which cross-sectional area tend to zero are heavily penalized by the optimizer. In that way, even when the topology evolves during the iterations of the SLP, removed members are hardly reintroduced in the optimization. To allow suppressed member to reappear in the optimized structure we apply a reinjection heuristic strategy. The a_j^0 value is updated every 30 SLP iterations inside Eq. 6 as follows:

$$a_j^0 = \max\left(a_j^0, \frac{1}{10}\max\left(\boldsymbol{a}^{\boldsymbol{0}}\right)\right). \tag{8}$$

This step reintroduces periodically many suppressed members and helps avoid local minima as shown later in the document.

Once convergence of Problem $\mathbb{P}_2$ is reached, the solution is used to simplify the initial ground structure, removing the elements in which $a < \max(\boldsymbol{a}) \times tol$. The physical cross-sectional member areas $\tilde{a}^*$ are retrieved using Eq. 2. The *tol* parameter is set to 10^{-3} in our analysis.

The next step is to set up the FEA of the updated ground structure to evaluate $\tilde{U}^*$. The linear system to solve for a truss is then:

$$\boldsymbol{f} = \boldsymbol{B}^T \boldsymbol{q} = \boldsymbol{B}^T \boldsymbol{D}\boldsymbol{\varepsilon} = \boldsymbol{B}^T \boldsymbol{D}\boldsymbol{B}\boldsymbol{U} = \boldsymbol{K}\boldsymbol{U}, \tag{9}$$

where $\boldsymbol{D} = \text{diag}\,(E\tilde{a}_i^*/\ell_i)$ and the stiffness matrix $\boldsymbol{K} = \boldsymbol{B}^T\boldsymbol{D}\boldsymbol{B}$.

Later, $\tilde{a}^*, \tilde{q}^*$ and $\tilde{U}^*$ are used as the starting point of the full NLP formulation where the kinematic compatibility and the exact local buckling formulation are restored. The solver finally outputs the optimized structure variables a^*, q^*, U^*.

In this work, we used the python library CVXPY[17] with the MOSEK solver to solve the relaxed LP problem $\mathbb{P}_2$. The full NLP problem $\mathbb{P}_1$ is instead solved using IPOPT[18], a large-scale nonlinear optimization package. The Jacobian and the Hessian matrices of the problem $\mathbb{P}_1$ are calculated at every optimization step to allow faster convergence. As every state variable of the optimization is independent of the others, these responses are easy to calculate and will not be detailed there.

III. Application to a cellular wing box

The proposed method is evaluated on a simplified 3D wing box. We simulate a drone wing box with an Aspect Ratio (AR) of 11 and dimensions of $\boldsymbol{L} = [5500\text{ mm}, 500\text{ mm}, 125\text{ mm}]$. The applied aerodynamic loads are the simultaneous application of lift and distributed torque that simulate the pitching moment. The lift is assumed as an elliptical distribution on the span-wise direction x and uniform distribution on the chord-wise direction y as such :

$$q(x) = q_{\max}\sqrt{1 - \left(\frac{x}{L_x/2}\right)^2}, \tag{10}$$

where $q_{\max} = \frac{4n_z Mg}{\pi L_x} = 1130$ N/m, if we assume $n_z = 1$, and $M = 1000$ kg.

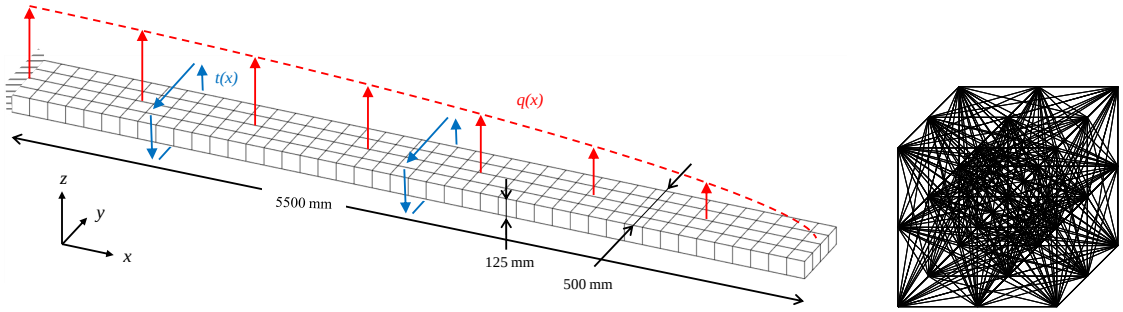

(a) (b)

Figure 4: (a) represents the 3D wing box discretized by 44×4×1 cells with lift (red forces) and torque (blue forces) applied. (b) shows the 351 members of a 3×3×3 fully connected ground structure. The cubic cell shown here can be stretched to accommodate non-cubic shapes.

Material	Aluminum alloy
E	69 GPa
σ_c	-270 MPa
σ_t	270 MPa
ρ	2.7 g/cm^3

Table 1: Elastic material properties used for the optimization.

The pitching torque is calculated using the panel method assuming inviscid and incompressible flow. The torque is written as a linear distribution on the span-wise direction x:

$$t(x) = t_{\max}\left(1 - \frac{x}{L_x}\right), \tag{11}$$

where $t_{max} = 0.208$ [N/m]. We notice that for a wing with a such AR, the pitching moment is almost negligible compared to the lift.

We also assume that the aerodynamic loads are not influenced by the deflection of the structure i.e., we neglect the aeroelastic interaction between fluid and structure. All the loads are applied statically. The load case is graphically represented, in Fig. 4a. The material used for the optimization is an aluminum alloy whose properties are schematized in Table 1.

The wing box is discretized in three different ways to investigate how the solution varies depending on the input parameters. We first conduct an optimization subdividing the wing box into 11×4×1 equal cells with dimensions of 500×125×125 mm each. Subsequently, the structure is discretized by 44×4×1 cubic cells with an edge length of 125 mm to investigate how the shape and the size of the repeating cell influence the optimized solution. Ultimately, the wing box is discretized by 44×4×1 octet-truss cells with fixed topology, comparing the advantages and disadvantages of the two approaches.

Every cell being optimized by the TTO algorithm is discretized by $m = 3x3x3$ equally spaced nodes that support a fully connected ground structure of 351 members (see Fig. 4b for a cubic representation of the cell ground structure). For simplicity, no influence of skin is taken into account in this study. The loads are applied on the center node of the upper face of the cells.

A. 11x4x1 cells TTO wing box

The wing box presented in Fig. 4a is subdivided into 11×4×1 equal cells with dimensions of 500×125×125 mm each. Doing that way, we obtain a span-wise distribution of cells that is comparable with the span-wise ribs distance of a classic wing design.

The optimized structure can be seen in Fig. 5, while Fig. 6 shows the topology of one cell. The suggested design is made by long spar-like elements well visible in Fig. 5c orthogonally cut by ribs formed by diagonally connected squares (see Fig. 5b and Fig. 6b). The lower part of the structure works, as expected, in tension, while the upper part in compression. As the optimization is buckling constrained, one can note that the compression members are more massive than tension ones (see Fig. 6a) with a maximum cross-sectional area of 325 mm^2. The final mass of the structure is 24.940 kg.

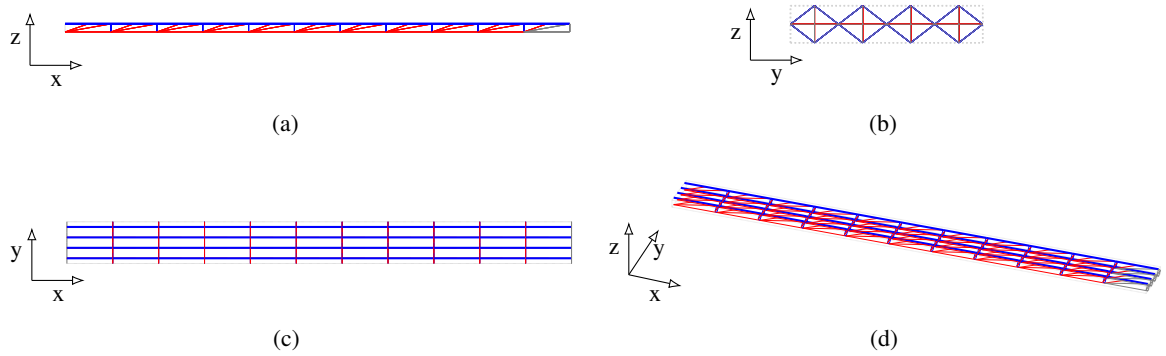

Figure 5: Orthogonal and perspective views of the 11×4×1 cells optimized topology. (a) shows the *xz* view (b) shows the *yz* view (c) shows the *xy* view and (d) shows the perspective view. Blue bars are loaded in compression, red ones are loaded in tension, while gray ones are unloaded. The cells create a complex structure that mimics the design of a classic wing with 4 spars- and 11 ribs-like substructures. (b) is enlarged 4 times to better display the topology to the reader.

Figure 7 shows the convergence history of the analysis, pointing out the difference between the LP and the NLP iterations. It is interesting to see that the reinjection strategy for local buckling used in the LP optimization permit to "jump" across a local minimum to land on a more interesting solution. We see that all the compressed bars of the web of the first topology are substituted by tension bars and a square with a tension diagonal in the second topology (see Fig. 6). Prioritizing the bars in tension, the second topology achieves a lower mass. In that example, the NLP only slightly modify the mass (+0.2%) of the LP solution because the cell topology is not statically indeterminate.

B. 44x4x1 cells TTO wing box

To investigate the effect of the cell size on the solution, we run another optimization subdividing the structure into 44×4×1 cubic cells with an edge length of 125 mm.

The optimized topology shows long 2D spars made by the repeating cell drawn in Fig. 8a. The topology is

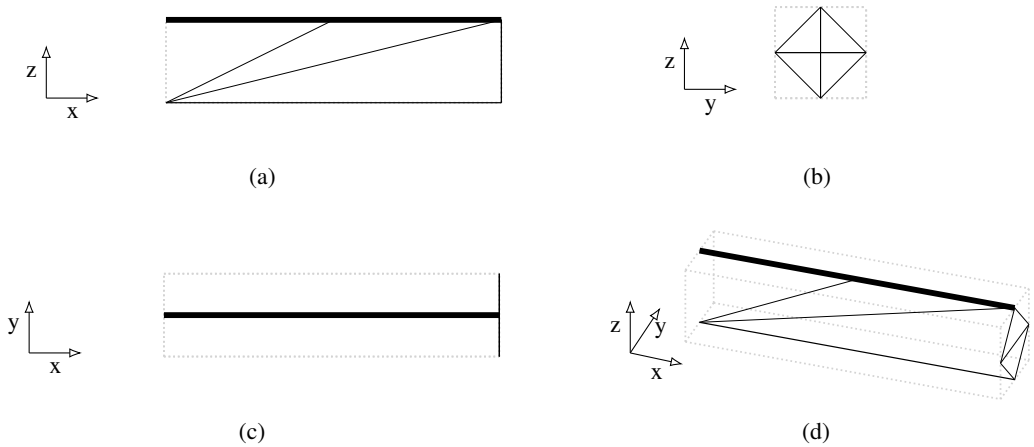

Figure 6: Orthogonal and perspective views of the optimized cell for the 11×4×1 wing box subdivision. (a) shows the *xy* view (b) shows the *xy* view (c) shows the *xy* view and (d) shows the perspective view.

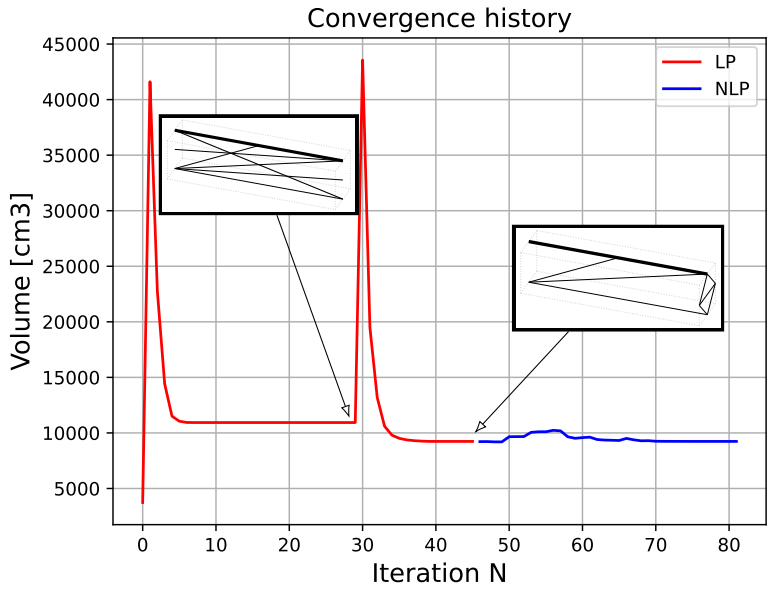

Figure 7: The volume of the structure is plotted against the optimizer iterations for the 11×4×1 TTO case. The plot shows the LP run in red, followed by the NLP in blue. The graph points out the efficiency of the reinjection strategy used in the LP at iteration 30 to avoid local minima.

similar to the 11×4×1 case, with a big compression member in the upper part of the cell, connected by thin tension bars to the lower part of the cell. The square sub-structure on yz plane of the previous solution (shown in Fig. 6b) is here rearranged into a single 2D column.

The 2D topology of the proposed solution should not be able to withstand the torque loads. However, the force-equilibrium constraint of the optimization is fully satisfied. The 2D structure is generated by a numeric artifact. To suppress the numeric noise of the solution at the end of the optimization, the members are thresholded with a value of $r = \max(\boldsymbol{a}) * 10^{-5}$. It turns out that, due to the low value of the applied torque with respect to the lift, the bars responsible for equilibrium in the y direction are suppressed.

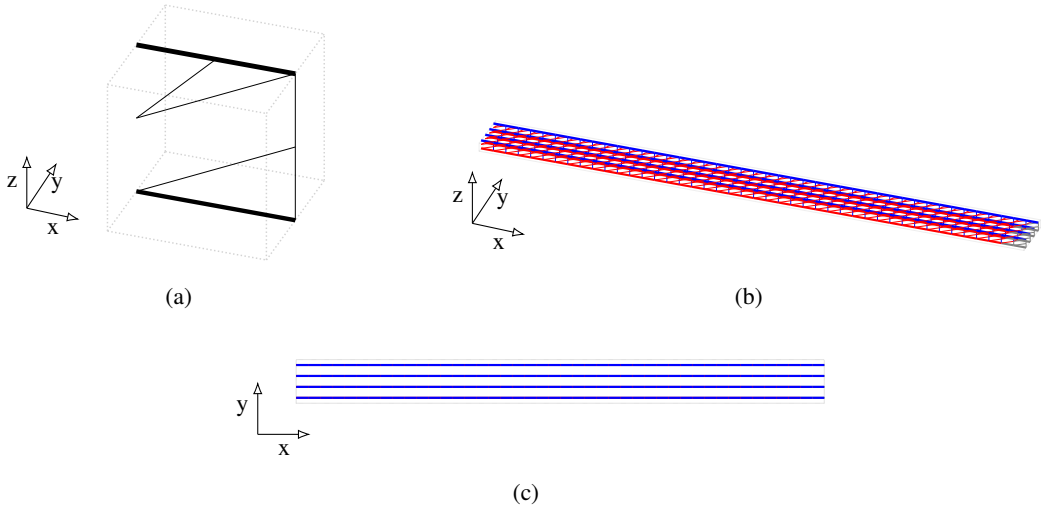

Figure 8: Orthogonal and perspective views of the 44×4×1 cells optimized topology. (a) shows the perspective view of the optimized cell. (b) shows the perspective view of the complete wing box. (c) shows the xy view of the complete wing box. Blue bars are loaded in compression, red ones are loaded in tension, while gray ones are unloaded.

Figure 9 presents the convergence history of the optimizing algorithm. We can see here again that the reinjection strategy used permits to avoid a local minimum.

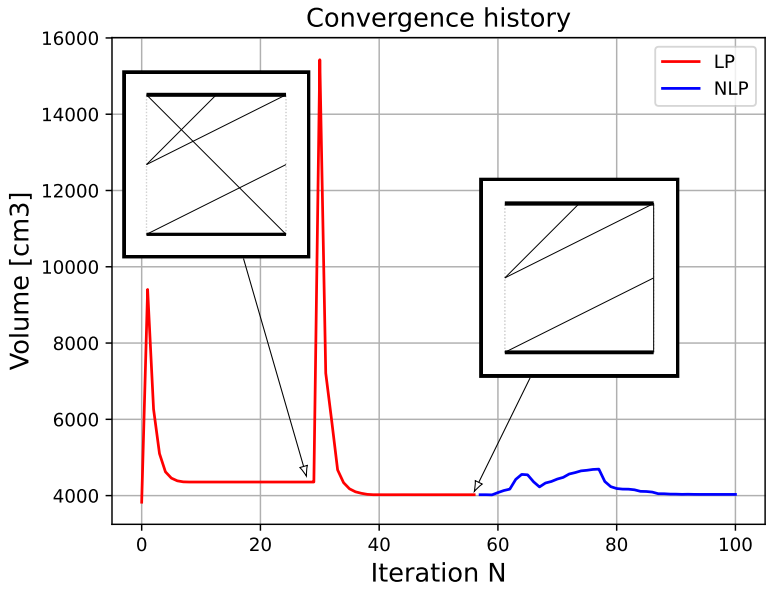

Figure 9: The volume of the structure is plotted against the optimizer iterations for the 44×4×1 TTO case. The plot shows the LP run in red, followed by the NLP in blue. The graph points out the efficiency of the reinjection strategy used in the LP at iteration 30 to avoid local minima.

C. 44x4x1 cells octet-truss wing box

The TTO algorithm is here benchmarked against one of the most popular cell topologies present in the literature: the octet-truss (see Fig. 10b). The octet-truss is a cell known for having very good effective mechanical properties that attain about half the theoretical values of the upper Hashin–Shtrikman bounds[19].

To perform the benchmark, the wing box of Figure 4a is meshed using 44×4×1 octet-truss cells of 125 mm of edge size (see Fig. 10). The cross-sectional areas of the cell members are all equal. The section value is evaluated by performing a parametric optimization on this section value, constrained by stress and local buckling for every member of the structure. The optimization is performed using Altair OptiStruct.

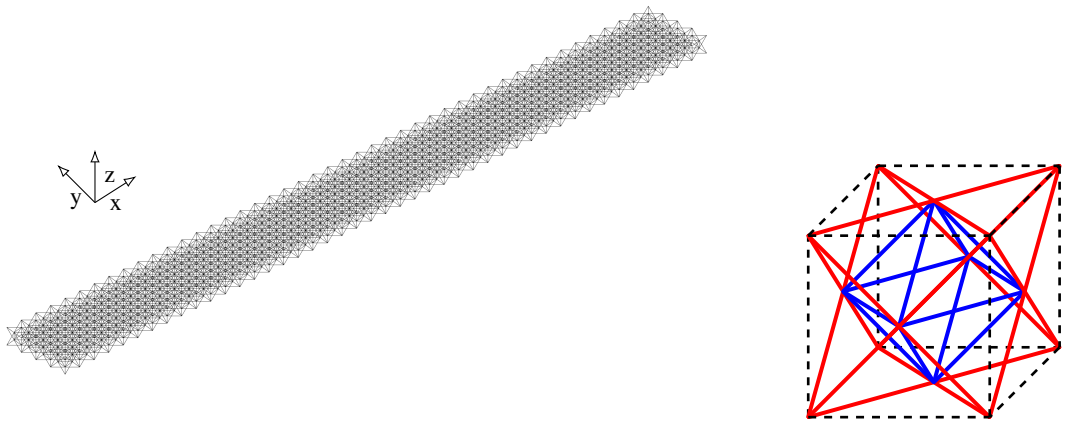

(a) (b)

Figure 10: (a) shows the OptiStruct mesh for the 44×4×1 octet-truss cells. (b) displays the unit octet-truss cell with blue struts representing the cuboct lattice bounded by 8 edge tetrahedrons (in red).

The optimized section value found is 85.027 mm, that is almost the same values of the maximum of the 44×4×1 TTO solution. The final optimized weight of the octet-truss case is 103.893 kg.

D. Discussion

The numerical results of the three tested cases are presented in Table 2. Some interesting conclusions can be drawn if we first compare the 11×4×1 TTO with the 44×4×1 TTO case, and later the 44×4×1 TTO with the octet-truss case.

Cell type	**Repetitions**	**Cell size** [mm]	**Mass** [kg]	**Compliance** [J]	**Tip deflection** [mm]	**Maximum area** [mm2]
TTO	11×4×1	500×125×125	24.940	585.248	356	325.327
TTO	44×4×1	125×125×125	10.867	782.138	467	87.093
Octet-truss	44×4×1	125×125×125	103.893	876.269	977	85.027

Table 2: Performance of the optimized designs with a different tassellation strategy.

We start observing again the topologies of the two TTO-optimized structures in Fig. 6d and Fig. 8a. The main difference between the two structures is that the section of the upper and the lower members, charged in compression and tension, is now comparable. This is due to the smaller length of the members of the 44×4×1 case and the subsequent change of failure mode of the compression member from local buckling to stress. Because of this more efficient use of the material, the final weight of the 44×4×1 structure is less than half of the 11×4×1 structure.

When using the variable linking scheme, the optimization problem becomes more and more constrained the more cells we put in the domain. One would expect to have better performances when using fewer cells. But in our case, this is not true. This is due to the fact that, even if the cell discretization remained the same for the two optimizations (3×3×3 nodes with a fully connected ground structure), the final ground structures are not the same. This is especially important as we saw that the 44×4×1 case ground structure is made up of smaller bars that help maximize the structure efficiency with respect to the buckling constraint.

One shortcoming of the two TTO-optimized cell topologies is that they are mechanisms on their own, acting as a structure only once connected with the other cells.

Comparing now the weight of the TTO and the octet-truss topologies is lighter by almost one order of magnitude. This big gap could be explained by two distinct observations:

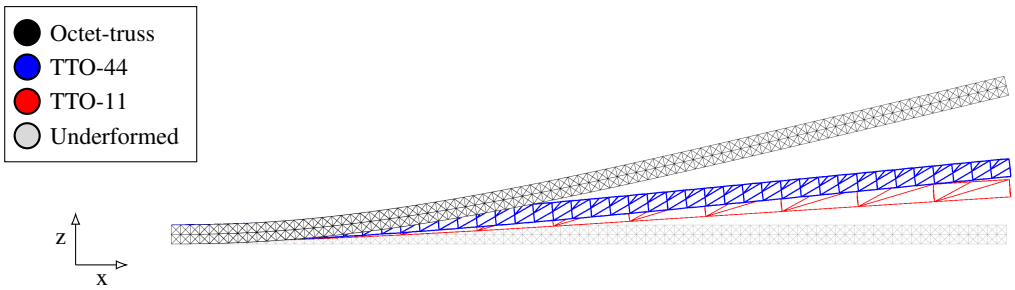

Figure 11: Comparison of the span-wise wing deflection of the three candidate structures. The TTO optimized solutions are more stiff and lighter than the octet-truss thanks to a more efficient topology of the cell.

1. We notice that in the octet-truss there are no members orientated exactly along the x axis, while in the TTO optimized cell they are the most massive. This clearly tells us that this is the most efficient direction to put the material to get a strong cell. On top of that, the upper and lower faces of the cell present a cross design (see Fig. 10b) that works well for torque but not for tension and compression loading. A new study exploring what happens if we rotate the cell could be interesting.

2. The octet-truss is a cell that exhibits good homogenized elastic properties in all directions thanks to its numerous plane of symmetry. It is, thus, less suitable for structural applications where all the cells present similar loading conditions, as the cell will be as stiff and strong in every direction and not aligned to the principal stress directions.

Nevertheless, the octet-truss is a stretching-dominated cell that is statically determined, and its manufacturability causes fewer issues than TTO-optimized cells.

It is important to note that the comparison that we are presenting here does not take into account the weight of fasteners and joints necessary to lint the cells together. In the case of the solution with 44 cells span-wise that weight would be multiplied by at least a factor of 4.

Finally, the deflection of the three wing boxes is represented in Fig. 11. Even being more massive, the wing tip deflection of the octet-truss case is almost double of the TTO. This is again due to the inefficient cross topology shown by the octet-truss cell in the upper and lower faces.

IV. Concluding remarks

This paper presents a comprehensive algorithm to optimize ultralight cellular structures. The classic LP formulation is extended to take into account an important mode of failure of trusses: local buckling. The repetitive aspect of the structure is implemented using the variable linking scheme as we suppose no scale separation between the structure and the repetitive pattern.

The optimization problem is solved using a two-step algorithm: we first solve a relaxed formulation by the means of SLP that is used to approximate the highly non-linear solution. Later, a full NLP formulation is solved where all the original constraints are restored. A reinjection numerical technique has been proposed to mitigate the appearance of local minima as well.

The proposed algorithm is applied to a real-size aerospace application, a cellular 3D wing box with a span of over 5 m. Compared to a classic cellular topology, the octet-truss, we saw a 10-times weight improvement, clearly showing the interest in cell optimization.

However, in the present form, TTO-optimized cells could present non-trivial shapes and questionable kinematic (mechanisms) that worsen the manufacturing phase, suggesting an interesting area of further research.

REFERENCES

[1] N. B. Cramer, D. W. Cellucci, O. B. Formoso, C. E. Gregg, B. E. Jenett, J. H. Kim, M. Lendraitis, S. S. Swei, G. T. Trinh, K. V. Trinh, and K. C. Cheung, "Elastic shape morphing of ultralight structures by programmable assembly," *Smart Materials and Structures*, vol. 28, p. 055006, Apr. 2019. Publisher: IOP Publishing.

[2] S. Zhou and Q. Li, "Design of graded two-phase microstructures for tailored elasticity gradients," *Journal of Materials Science*, vol. 43, pp. 5157–5167, Aug. 2008.

[3] J. Wu, O. Sigmund, and J. P. Groen, "Topology optimization of multi-scale structures: a review," *Structural and Multidisciplinary Optimization*, Mar. 2021.

[4] O. Sigmund, N. Aage, and E. Andreassen, "On the (non-)optimality of Michell structures," *Structural and Multidisciplinary Optimization*, vol. 54, pp. 361–373, Aug. 2016.

[5] G. Rozvany, "On design-dependent constraints and singular topologies," *Structural and Multidisciplinary Optimization*, vol. 21, pp. 164–172, Apr. 2001.

[6] N. Aage, E. Andreassen, B. S. Lazarov, and O. Sigmund, "Giga-voxel computational morphogenesis for structural design," *Nature*, vol. 550, pp. 84–86, Oct. 2017. Number: 7674 Publisher: Nature Publishing Group.

[7] M. A. Salazar de Troya and D. A. Tortorelli, "Adaptive mesh refinement in stress-constrained topology optimization," *Structural and Multidisciplinary Optimization*, vol. 58, pp. 2369–2386, Dec. 2018.

[8] W. S. Dorn, R. E. Gomory, and H. Greenberg, "Automatic design of optimal structures," *J. Mécanique*, 1964.

[9] G. Rozvany, M. P. Bendsøe, and U. Kirsch, "Layout Optimization of Structures," *Applied Mechanics Reviews*, vol. 48, pp. 41–119, Feb. 1995.

[10] K. F. Reinschmidt and A. D. Russell, "Applications of linear programming in structural layout and optimization," *Computers & Structures*, vol. 4, pp. 855–869, Aug. 1974.

[11] W. Achtziger, "Local stability of trusses in the context of topology optimization Part I: Exact modelling," *Structural Optimization*, vol. 17, pp. 235–246, Dec. 1999.

[12] M. Kočvara, "On the modelling and solving of the truss design problem with global stability constraints," *Structural and Multidisciplinary Optimization*, vol. 23, pp. 189–203, Apr. 2002.

[13] W. Zhang and S. Sun, "Scale-related topology optimization of cellular materials and structures," *International Journal for Numerical Methods in Engineering*, vol. 68, no. 9, pp. 993–1011, 2006. _eprint: https://onlinelibrary.wiley.com/doi/pdf/10.1002/nme.1743.

[14] E. Parkes, "Joints in optimum frameworks," *International Journal of Solids and Structures*, vol. 11, pp. 1017–1022, Sept. 1975.

[15] G. Cheng, "Some aspects of truss topology optimization," *Structural Optimization*, vol. 10, pp. 173–179, Dec. 1995.

[16] J. Schwarz, T. Chen, K. Shea, and T. Stanković, "Efficient size and shape optimization of truss structures subject to stress and local buckling constraints using sequential linear programming," *Structural and Multidisciplinary Optimization*, vol. 58, pp. 171–184, July 2018.

[17] S. Diamond and S. Boyd, "CVXPY: A Python-Embedded Modeling Language for Convex Optimization," 2016.

[18] A. Wächter and L. T. Biegler, "On the implementation of an interior-point filter line-search algorithm for large-scale nonlinear programming," *Mathematical Programming*, vol. 106, pp. 25–57, Mar. 2006.

[19] V. S. Deshpande, N. A. Fleck, and M. F. Ashby, "Effective properties of the octet-truss lattice material," *Journal of the Mechanics and Physics of Solids*, vol. 49, pp. 1747–1769, Aug. 2001.